Electronic Supplementary Material (ESI) for Chemical Communications.

Supplementary Information

Mechanochemical reactions of cocrystals: comparing theory with experiment in the making and breaking of halogen bonds in the solid state

Mihails Arhangelskis, Filip Topić, Poppy Hindle, Ricky Tran, Andrew J. Morris, Dominik Cinčić,* and Tomislav Friščić*

Table of Contents

1. Experimental details

All solvents used for syntheses and crystal growth were of reagent grade and were used as received. Tetrafluoro-1,2-diiodobenzene (**12tfib**) was purchased from Oakwood Products, Inc., while 1,4-diazabicyclo[2.2.2]octane (**dabco**) was purchased from Sigma-Aldrich.

Mechanochemical experiments were conducted on a Retsch MM200 mill operating at 25 Hz frequency using a pair of 15 mL polytetrafluoroethylene (PTFE) jars, each with a zirconia ball (10 mm diameter and 4 g weight).

Powder X-ray diffraction (PXRD) experiments were performed on a Bruker D8 Advance diffractometer, using a Cu*K*α (λ = 1.54184 Å) radiation source operating at 40 mA and 40 kV, equipped with a Lynxeye XE linear position sensitive detector, in the 2θ range of 4–40° with step size of 0.019° or, alternatively, on a Proto AXRD X-ray diffractometer, using a Cu*K*α (λ = 1.54184 Å) radiation source operating at 20 mA and 30 kV, equipped with a Dectris MYTHEN 1K one-dimensional linear detector, in the 2θ range of 4–40° with step size of 0.04°. Data analysis was performed using the program package Philips X'Pert.

Rietveld refinement of the PXRD patterns was performed using the Program Topas Academic 6 (Coelho software).[1] The background was modelled with a 6th degree polynomial function, and the peak shape was described by a pseudo-Voigt function. Crystal structures obtained from single crystal X-ray diffraction experiments were used in the refinement. The unit cell parameters were refined to account for the temperature effects, while the atomic coordinates remained fixed.

Thermal Analysis. Simultaneous TGA and DSC measurements were performed using a Mettler-Toledo TGA/DSC 1 thermal analyzer in open alumina crucibles (70 µL), heated in a stream of nitrogen (50 mL min^{-1}) at a heating rate of 5 °C min^{-1} from 30 to 400 °C. Data collection and analysis were performed using the STARe Software 16.00 program package.[2]

Fourier-transform infrared attenuated total reflectance (FTIR-ATR) measurements were performed on a Bruker VERTEX 70 instrument equipped with a single-reflection diamond crystal Platinum ATR unit.

2. Periodic DFT calculations

Periodic DFT calculations were performed using a plane-wave DFT code CASTEP19.[3] The input files were generated from the experimental crystal structures using the program cif2cell.[4] Calculations were performed using a PBE[5] functional combined with many body dispersion (MBD*),[6–8] Grimme-D2[9] and Tkatchenko-Scheffler (TS)[10] corrections. Additional calculations were performed using LDA,[11] PBEsol[12] and PBE functionals without dispersion correction. The plane wave basis set was truncated at 800 eV cutoff, and ultrasoft pseudopotentials from the CASTEP library were used to model the core regions of electron density. The 1st electronic Brillouin zone was sampled with a 0.03 Å^{-1} Monkhorst-Pack[13] k-point grid.

The crystal structures of (**dabco**)(**12tfib**) cocrystals as well as pure crystalline **dabco** and **12tfib** were geometry-optimized subject to the symmetry constraints of the corresponding space groups. The optimization procedure involved relaxation of both unit cell parameters and atom coordinates. The calculations were deemed finished upon reaching the following convergence criteria: maximum energy change 2x10^{-5} eV/atom; maximum force on atom 0.05 eV Å^{-1}; maximum atom displacement 10^{-3} Å; maximum residual stress 0.1 GPa.

Finally, the computational cost of an average geometry optimization step was computed for each structure calculated with each method (Table S2). The time was averaged over five regular BFGS optimization steps, which include a trial and a line improvement step.

Table S1 Comparison of the calculated and experimental halogen bond lengths. All symmetry non-equivalent interactions are shown as separate numbers. In order to account for disorder in (**dabco**)(**12tfib**)-HT structure, the symmetry of the structure was reduced from *C*2/*c* to *P*1. Because of that, the simulated structure has four non-equivalent halogen bonds, while the experimental disordered structure has only one crystallographically distinct halogen bond.

Cocrystal	Calculated XB length / Å						Experimental XB length / Å
	PBE+MBD*	PBE+TS	PBE+D2	PBE	PBEsol	LDA	
(**dabco**)(**12tfib**)-HT	2.673; 2.701; 2.722; 2.820	2.728; 2.737; 2.773; 2.852	2.641; 2.657; 2.739; 2.772	2.752; 2.757; 2.793; 2.796	2.670; 2,673; 2.681; 2.699	2.576; 2.578; 2.611; 2.664	2.805(2)
(**dabco**)(**12tfib**)-LT	2.675; 2.695; 2.700; 2.785	2.767; 2.773; 2.783; 2.792	2.685; 2.686; 2.704; 2.717	2.768; 2.769; 2.769; 2.775	2.665; 2.672; 2.674; 2.679	2.582; 2.586; 2.597; 2.610	2.779(7); 2.780(7); 2.783(7); 2.794(7)
(**dabco**)(**12tfib**)$_2$	2.668; 2.709	2.713; 2.741	2.675; 2.702	2.746; 2.799	2.655; 2.673	2.573; 2.596	2.76(1); 2.80(1)
(**dabco**)$_2$(**12tfib**)	2.643; 2.743	2.796; 2.792	2.680; 2.683	2.741; 2.785	2.655; 2.692	2.552; 2.583	2.806(5); 2.822(5)

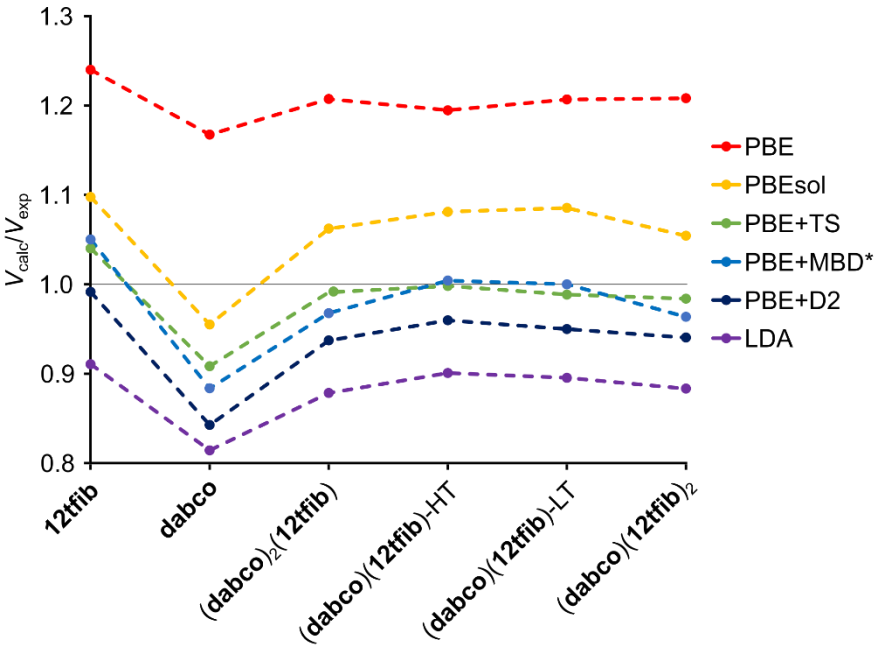

Fig. S1 Ratio of calculated and experimental unit cell volumes for starting materials and the herein reported cocrystal structures of **dabco** and **12tfib** using different methods: PBE, PBEsol, PBE+TS, PBE+MBD*, PBE+D2 and LDA.

Table S2 Computational cost of periodic DFT optimization for starting materials and the herein reported cocrystal structures of **dabco** and **12tfib** using different methods: PBE, PBEsol, PBE+MBD*, PBE+TS, PBE+D2 and LDA.

Structure	**CPU time / hours[a]**					
	PBE+MBD*	**PBE+D2**	**PBE+TS**	**PBE**	**LDA**	**PBEsol**
1,2-tfib	4.6(1)	2.8(1)	2.8(2)	3.3(3)	3.2(2)	3.3(3)
dabco	9.3(5)	1.2(2)	1.1(2)	1.2(2)	0.8(1)	1.1(2)
(**dabco**)(**1,2-tfib**)-HT	19.5(2)	8.3(1)	8.0(7)	9(1)	8.7(5)	8.0(3)
(**dabco**)(**1,2-tfib**)-LT	32.4(3)	16.1(9)	17(1)	19(2)	17.3(4)	16(1)
(**dabco**)(**1,2-tfib**)$_2$	11.1(2)	6.4(3)	6.6(3)	8(1)	6.9(2)	7.0(6)
(**dabco**)$_2$(**1,2-tfib**) disordered configuration 1	13.0(4)	8.4(4)	8.2(4)	8.5(5)	8.1(5)	8.1(7)
(**dabco**)$_2$(**1,2-tfib**) disordered configuration 2	13.0(5)	8.6(6)	8.4(4)	8.4(7)	8.1(4)	8.0(6)

a) Relative computational cost of various methods was calculated by comparing the time it takes to perform one geometry optimization step with each method for every crystal structure.

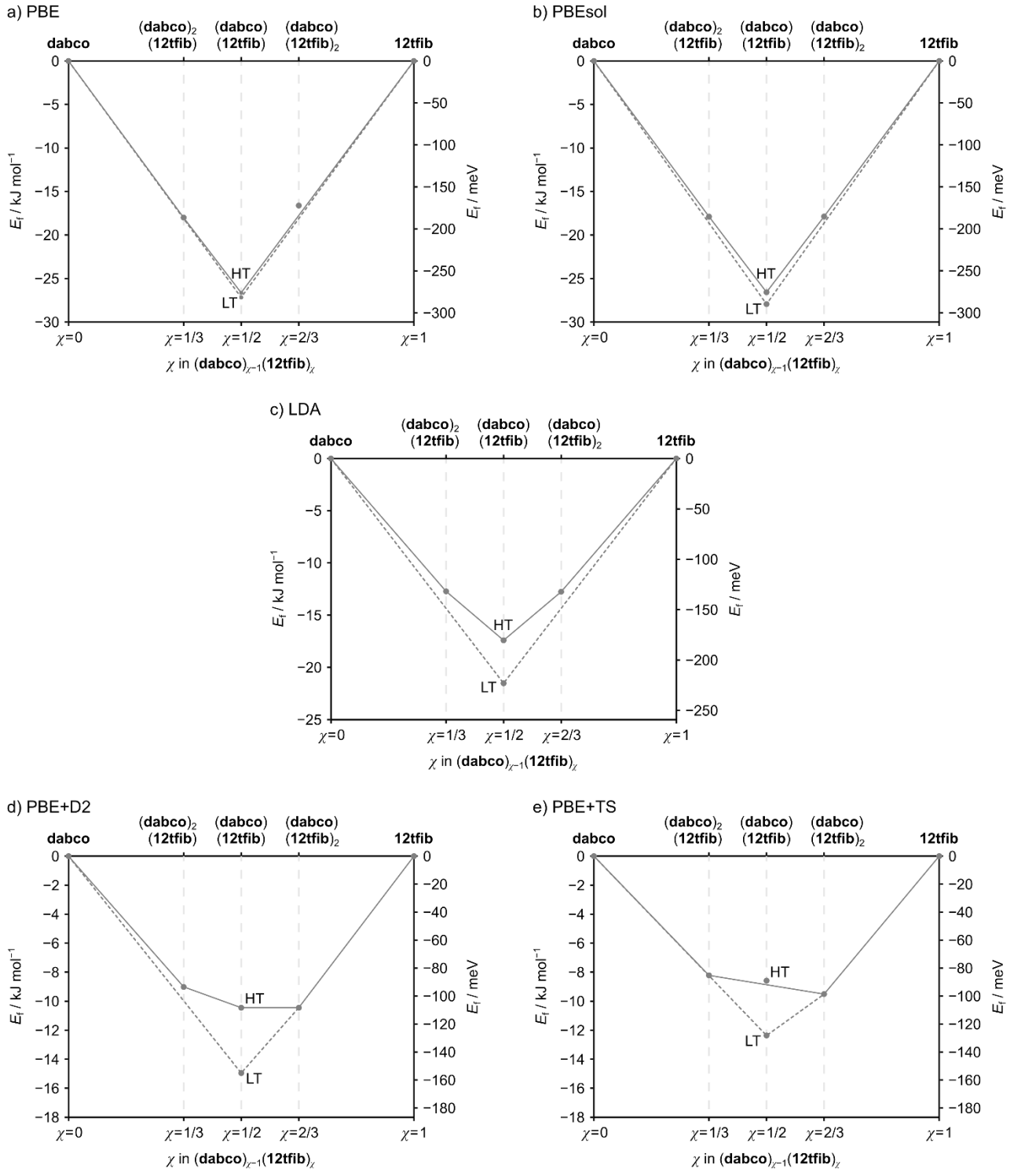

Fig. S2 Formation energy of cocrystals as a function of **dabco** : **12tfib** stoichiometric ratio, using different functionals a) PBE, b) PBEsol, c) LDA, d) PBE+D2 and e) PBE+TS. The convex hull drawn with a solid line includes the monoclinic (**dabco**)(**12tfib**)-HT form, whereas the triclinic (**dabco**)(**12tfib**)-LT form is connected by a dashed line.

3. Preparation of the cocrystals

(**dabco**)$_2$(**12tfib**):
A mixture of **dabco** (107.6 mg, 0.9592 mmol) and **12tfib** (192.5 mg, 0.4790 mmol) was placed in a PTFE jar along with a zirconia ball and 30 μL of nitromethane. The mixture was then milled for 15 min.

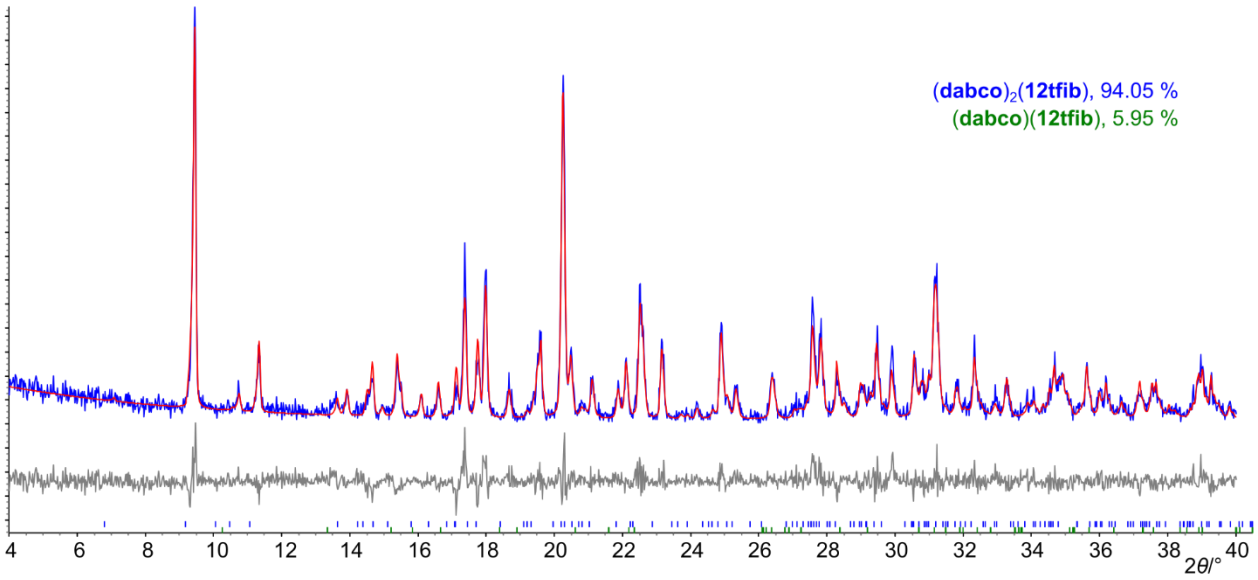

Fig. S3 Rietveld plot for a mechanochemically prepared sample of (**dabco**)$_2$(**12tfib**), showing the presence of ~6 % of (**dabco**)(**12tfib**) as an impurity. Calculated, experimental and difference PXRD patterns are shown respectively in red, blue and grey.

(**dabco**)(**12tfib**):
A mixture of **dabco** (65.6 mg, 0.585 mmol) and **12tfib** (234.5 mg, 0.5835 mmol) was placed in a PTFE jar along with a zirconia ball and 30 μL of nitromethane. The mixture was then milled for 15 min.

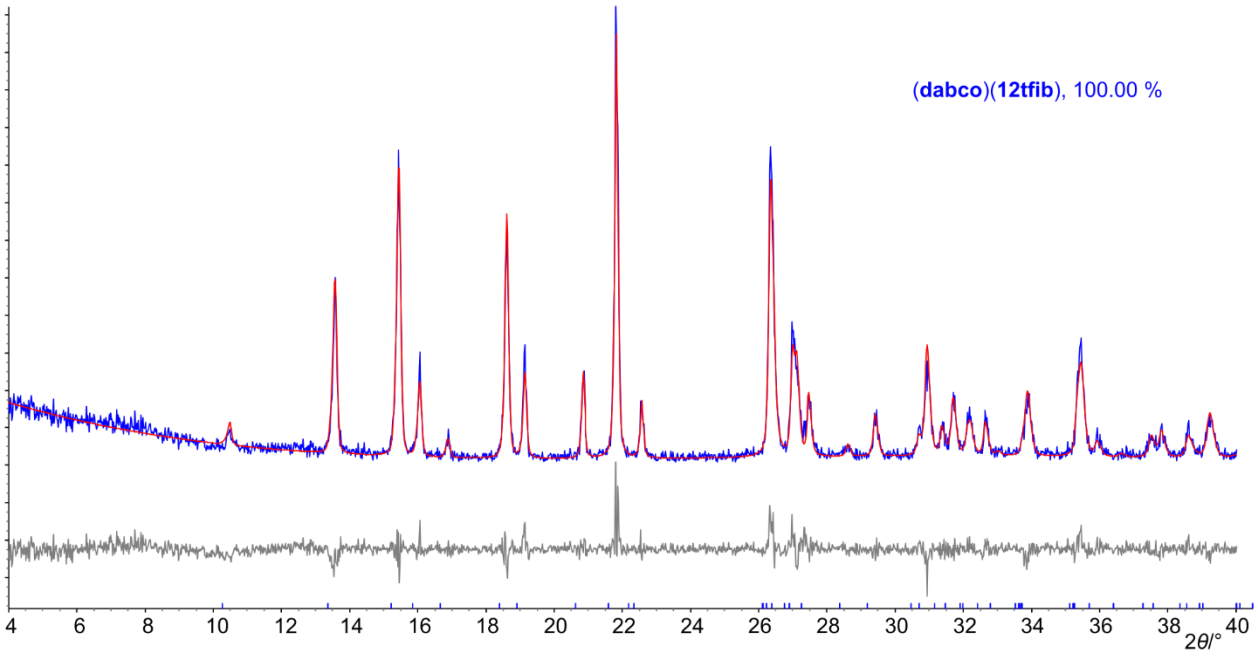

Fig. S4 Rietveld plot for a mechanochemically prepared sample of (**dabco**)(**12tfib**). Calculated, experimental and difference PXRD patterns are shown respectively in red, blue and grey.

(**dabco**)(**12tfib**)$_2$:
A mixture of **dabco** (36.8 mg, 0.328 mmol) and **12tfib** (263.3 mg, 0.6552 mmol) was placed in a PTFE jar along with a zirconia ball and 30 µL of nitromethane. The mixture was then milled for 15 min.

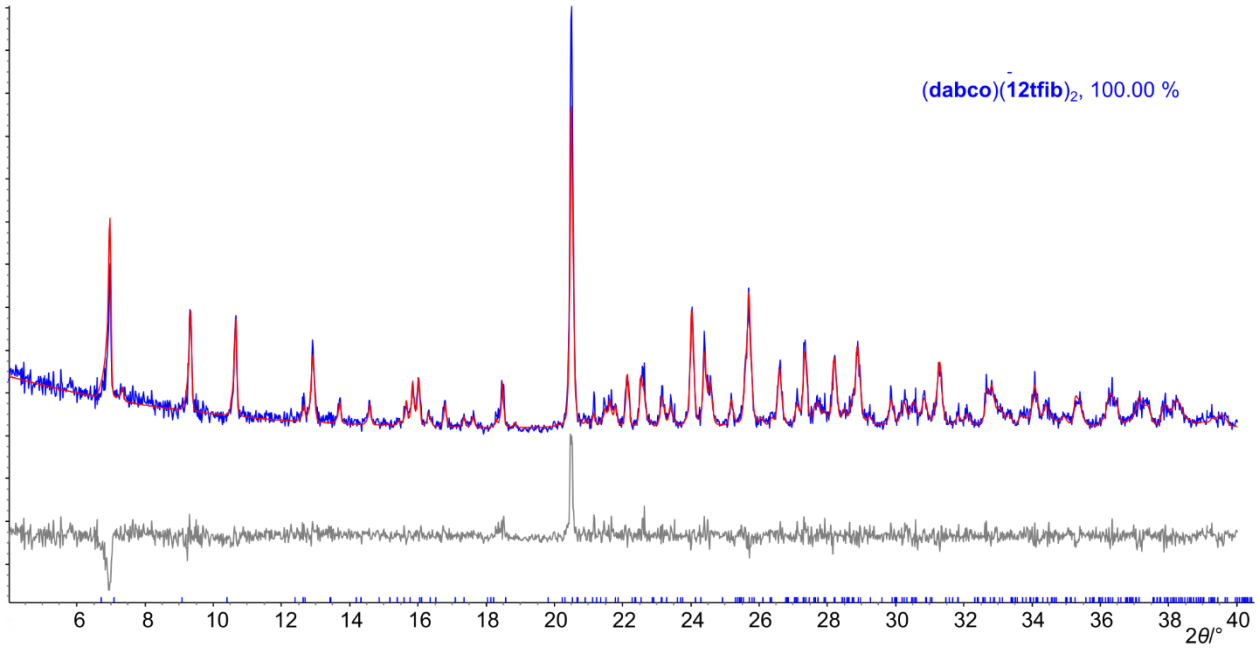

Fig. S5 Rietveld plot for a mechanochemically prepared sample of (**dabco**)(**12tfib**)$_2$. Calculated, experimental and difference PXRD patterns are shown respectively in red, blue and grey.

4. Single crystal growth

(**dabco**)$_2$(**12tfib**):
Single crystals were obtained upon evaporation of a solution obtained by dissolving **dabco** (15.1 mg, 0.135 mmol) and **12tfib** (13.4 mg, 0.0333 mmol) in 0.2 mL acetone with heating.

(**dabco**)(**12tfib**):
Single crystals were obtained upon cooling of a solution obtained by dissolving a solid sample of (**dabco**)(**12tfib**) (71.7 mg, 0.139 mmol) in 0.75 mL nitromethane with heating, seeded with a spatula-tip of (**dabco**)(**12tfib**) obtained mechanochemically.

(**dabco**)(**12tfib**)$_2$:
Single crystals were obtained upon evaporation of a solution obtained by dissolving a solid sample of (**dabco**)(**12tfib**)$_2$ (70.8 mg, 0.0773 mmol) in a mixture of 0.8 mL ethanol and 0.1 mL water with heating.

5. Interconversion experiments

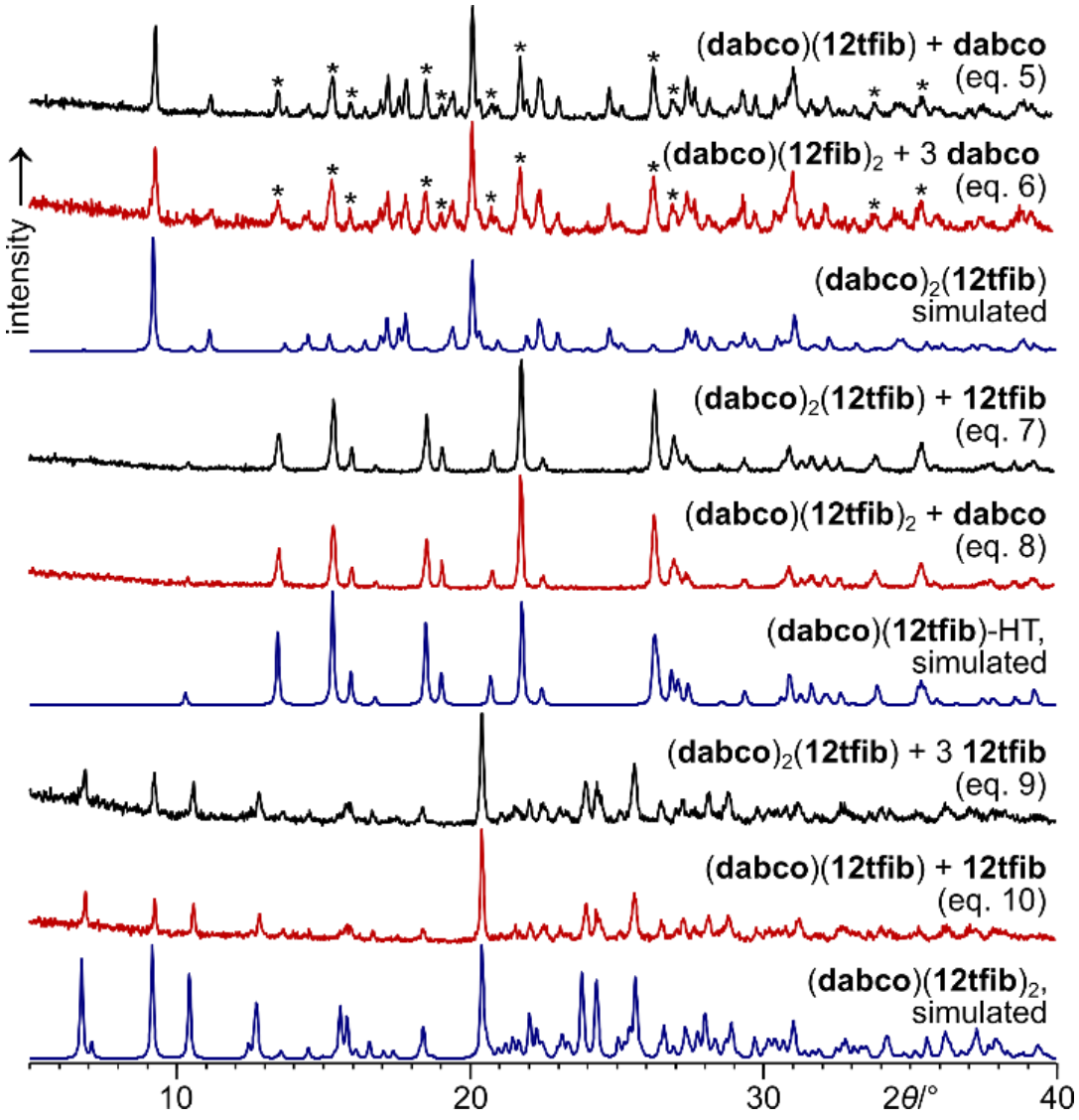

Fig. S6 Overlay of PXRD patterns for mechanochemical reaction mixtures corresponding to eqn (5)–(10) in the manuscript. The reactions were prepared by LAG of corresponding starting materials for 15 minutes. Bragg reflections corresponding to the traces of (**dabco**)(**12tfib**)-HT in samples of (**dabco**)$_2$(**12tfib**) are marked by asterisks (*).

(**dabco**)(**12tfib**) + **dabco**:
A mixture of (**dabco**)(**12tfib**) (164.2 mg, 0.3194 mmol) and **dabco** (36.0 mg, 0.321 mmol) was placed in a PTFE jar along with a zirconia ball and 30 µL of nitromethane. The mixture was then milled for 15 min.

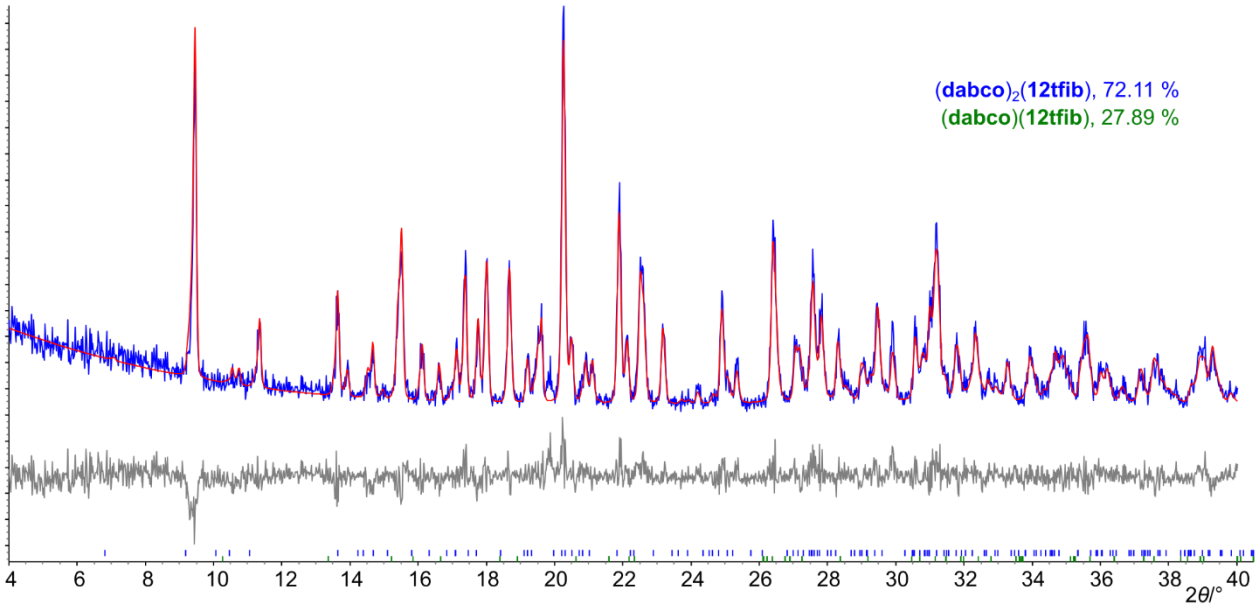

Fig. S7 Rietveld plot for a sample obtained by the mechanochemical reaction (**dabco**)(**12tfib**) + **dabco**. Calculated, experimental and difference PXRD patterns are shown respectively in red, blue and grey.

(**dabco**)(**12tfib**)$_2$ + 3 **dabco**:
A mixture of (**dabco**)(**12tfib**)$_2$ (146.3 mg, 0.1597 mmol) and **dabco** (53.7 mg, 0.479 mmol) was placed in a PTFE jar along with a zirconia ball and 30 µL of nitromethane. The mixture was then milled for 15 min.

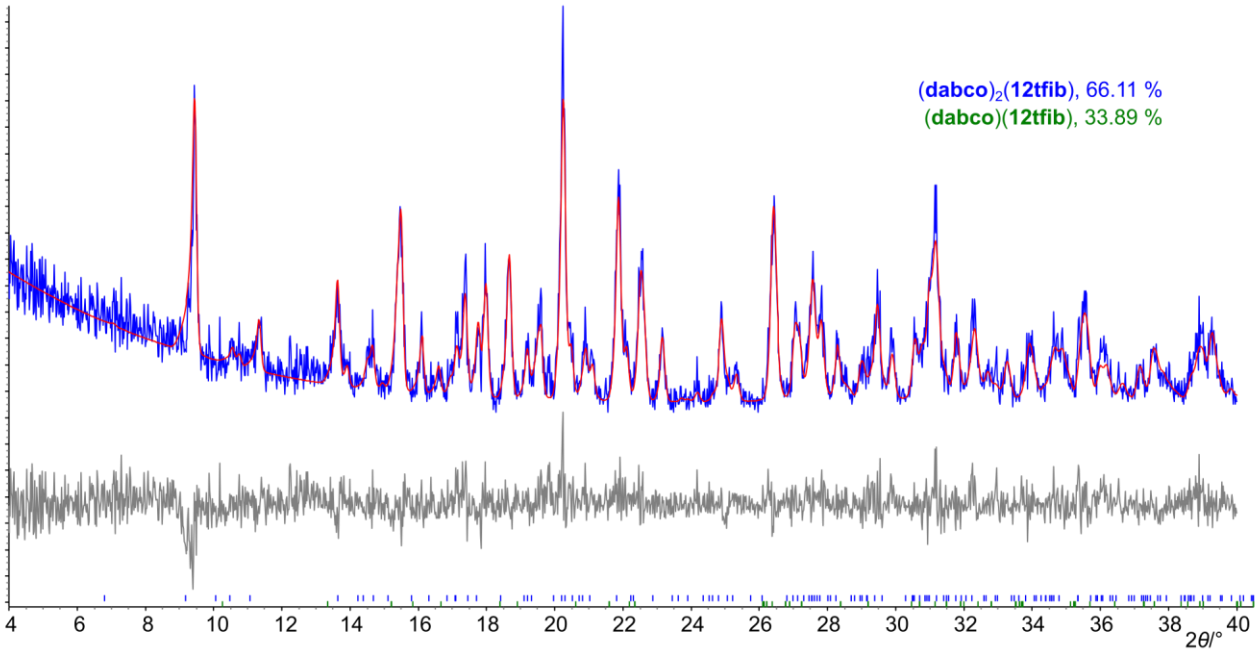

Fig. S8 Rietveld plot for a sample obtained by the mechanochemical reaction (**dabco**)(**12tfib**)$_2$ + 3 **dabco**. Calculated, experimental and difference PXRD patterns are shown respectively in red, blue and grey.

(**dabco**)$_2$(**12tfib**) + **12tfib**:
A mixture of (**dabco**)$_2$(**12tfib**) (121.8 mg, 0.1945 mmol) and **12tfib** (78.2 mg, 0.195 mmol) was placed in a PTFE jar along with a zirconia ball and 30 µL of nitromethane. The mixture was then milled for 15 min.

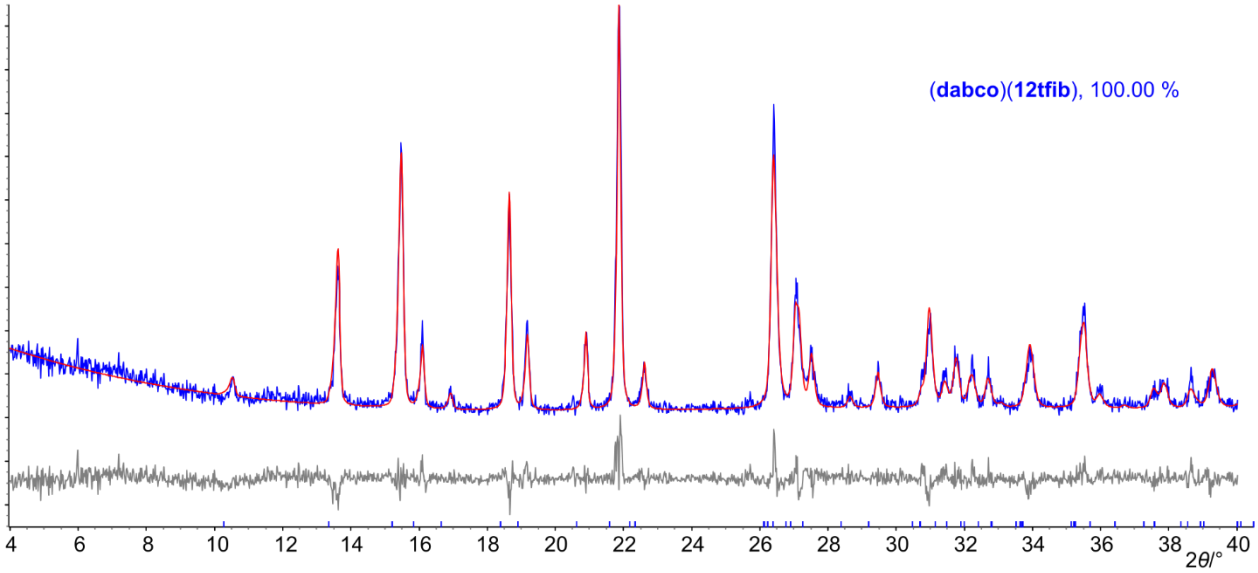

Fig. S9 Rietveld plot for a sample obtained by the mechanochemical reaction (**dabco**)$_2$(**12tfib**) + **12tfib**. Calculated, experimental and difference PXRD patterns are shown respectively in red, blue and grey.

(**dabco**)(**12tfib**)$_2$ + **dabco**:
A mixture of (**dabco**)(**12tfib**)$_2$ (178.2 mg, 0.1946 mmol) and **dabco** (21.9 mg, 0.195 mmol) was placed in a PTFE jar along with a zirconia ball and 30 µL of nitromethane. The mixture was then milled for 15 min.

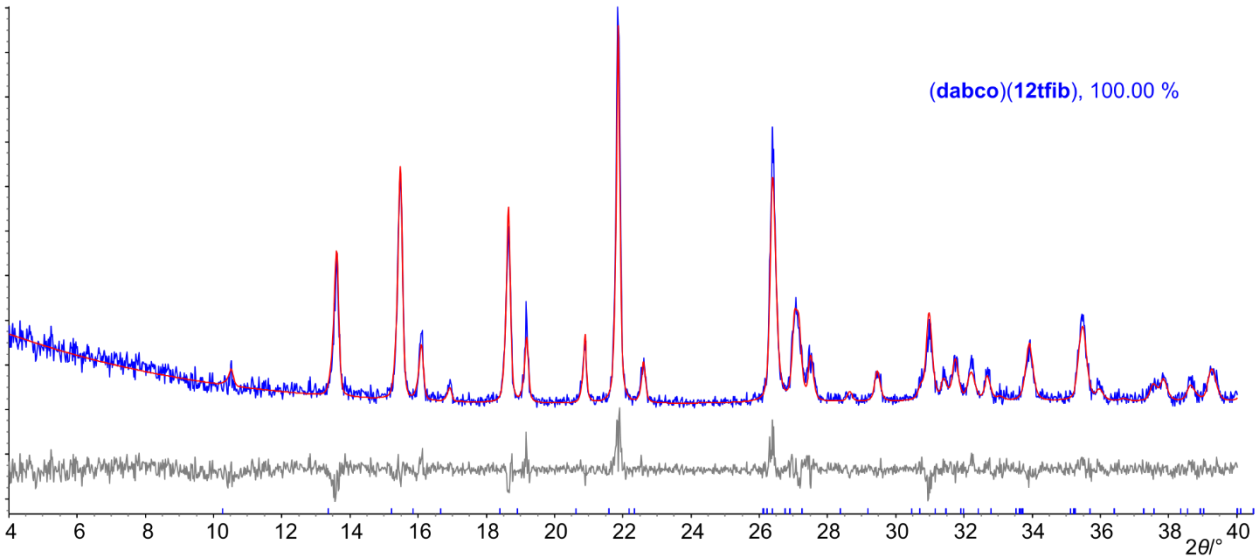

Fig. S10 Rietveld plot for a sample obtained by the mechanochemical reaction (**dabco**)(**12tfib**)$_2$ + **dabco**. Calculated, experimental and difference PXRD patterns are shown respectively in red, blue and grey.

(**dabco**)$_2$(**12tfib**) + 3 **12tfib**:
A mixture of (**dabco**)$_2$(**12tfib**) (68.4 mg, 0.109 mmol) and **12tfib** (131.7 mg, 0.3277 mmol) was placed in a PTFE jar along with a zirconia ball and 30 µL of nitromethane. The mixture was then milled for 15 min.

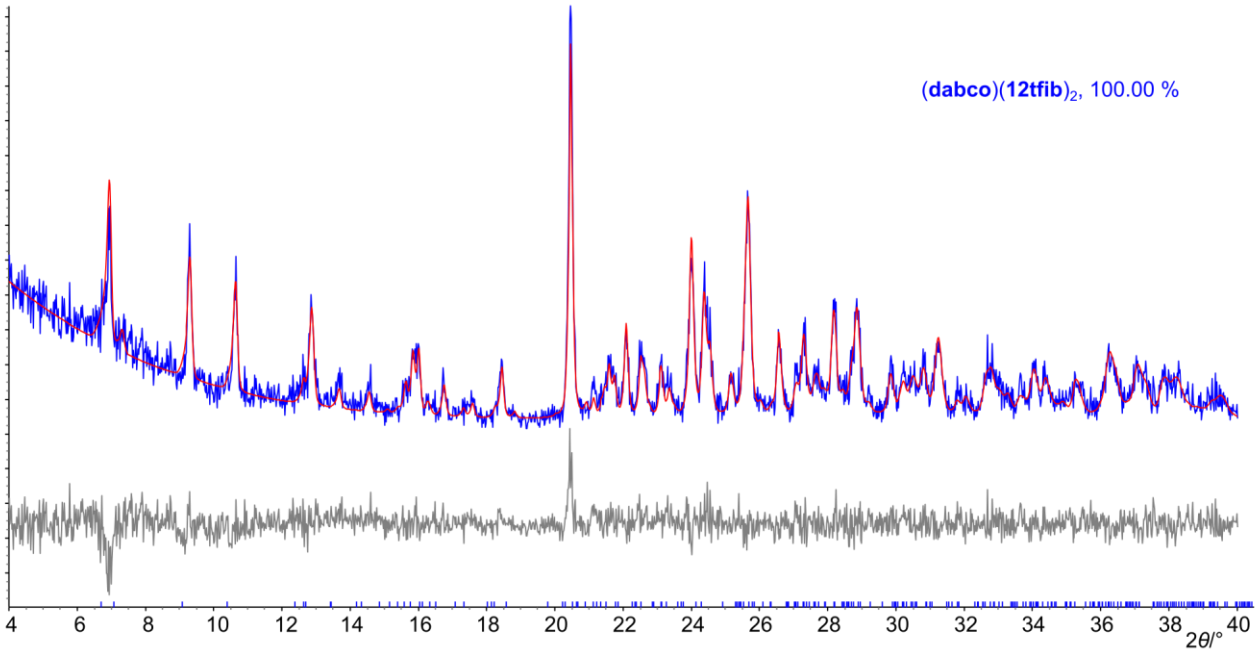

Fig. S6 Rietveld plot for a sample obtained by the mechanochemical reaction (**dabco**)$_2$(**12tfib**) + 3 **12tfib**. Calculated, experimental and difference PXRD patterns are shown respectively in red, blue and grey.

(**dabco**)(**12tfib**) + **12tfib**:
A mixture of (**dabco**)(**12tfib**) (112.2 mg, 0.2183 mmol) and **12tfib** (87.9 mg, 0.219 mmol) was placed in a PTFE jar along with a zirconia ball and 30 µL of nitromethane. The mixture was then milled for 15 min.

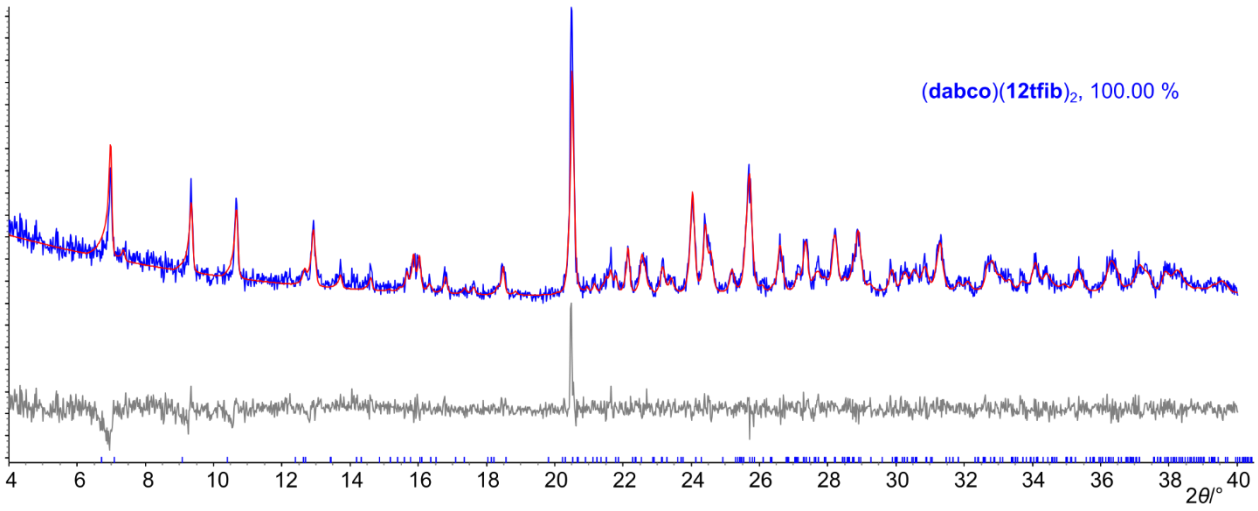

Fig. S7 Rietveld plot for a sample obtained by the mechanochemical reaction (**dabco**)(**12tfib**) + **12tfib**. Calculated, experimental and difference PXRD patterns are shown respectively in red, blue and grey.

6. Crystal structure determinations

Single crystal X-ray diffraction data were collected at 253 K on a Bruker D8 Venture dual-source diffractometer equipped with a PHOTON 100 or PHOTON II detector and an Oxford Cryostream 800 cooling system, using mirror-monochromatized Mo*K*α (λ = 0.71073 Å) or Cu*K*α (λ = 1.54184 Å) radiation from respective microfocus sources. Data were collected in a series of φ- and ω-scans. APEX3 software was used for data collection, integration and reduction.[14] Semi-empirical absorption correction was applied using SADABS-2016/2.[15]

Structures were solved by dual-space iterative methods using SHELXT-2014/5 or SHELXT-2018/2[16] and refined by full-matrix least-squares on F^2 using all data with SHELXL-2017/1 or SHELXL-2018/3[17] within OLEX2 and WinGX[18] packages. All non-hydrogen atoms were refined anisotropically. Hydrogen atoms were placed in calculated positions and treated as riding on the parent carbon atoms with U_{iso}(H) = 1.2 U_{eq}(C). Extinction correction was applied as implemented in SHELXL-2018/3.[17] Crystal structure figures were generated using Mercury[19] and POV-Ray.[20]

(**dabco**)(**12tfib**)-HT was found to be pseudomerohedrally twinned, with two-components related by a two-fold rotation around the (0 0 1) reciprocal lattice direction. This was accounted for in the refinement, and the batch scale factor was refined, converging to 0.1371(5).

CCDC 1990460–1990463 contain the supplementary crystallographic data for this paper. The data can be obtained free of charge from The Cambridge Crystallographic Data Centre via www.ccdc.cam.ac.uk/structures.

Table S3 Crystallographic data for the crystal structures presented in this work

Cocrystal	(**dabco**)$_2$(**12tfib**)	(**dabco**)(**12tfib**)-HT	(**dabco**)(**12tfib**)-LT	(**dabco**)(**12tfib**)$_2$
CCDC Number	1990462	1990460	1990463	1990461
Formula	$C_{18}H_{24}F_4I_2N_4$	$C_{12}H_{12}F_4I_2N_2$	$C_{12}H_{12}F_4I_2N_2$	$C_{18}H_{12}F_8I_4N_2$
M_r	626.21	514.04	514.04	915.90
T (K)	253.0(1)	253.0(1)	173.0(1)	253.0(1)
Crystal system	orthorhombic	monoclinic	triclinic	triclinic
Space group	$P2_12_12_1$	$C2/c$	$P\bar{1}$	$P\bar{1}$
a (Å)	6.5273(5)	8.4114(6)	6.7231(5)	7.5107(5)
b (Å)	17.4784(13)	11.1190(8)	14.0970(10)	12.8506(8)
c (Å)	19.2084(14)	17.6646(11)	17.5147(13)	13.4853(9)
α (°)	90	90	76.882(3)	94.235(2)
β (°)	90	103.661(3)	80.884(3)	102.514(2)
γ (°)	90	90	78.615(2)	102.883(2)
V (Å^3)	2191.4(3)	1605.37(19)	1573.6(2)	1228.41(14)
Z	4	4	4	2
ρ_{calc} (g cm^{-3})	1.898	2.127	2.170	2.476
μ (mm^{-1})	2.914	3.949	31.730	5.143
F(000)	1208	960	960	836
Crystal size (mm^3)	0.830×0.194×0.091	0.952×0.197×0.126	0.311×0.247×0.098	0.873×0.358×0.202
θ range for data collection (°)	3.152–33.197	4.746–31.057	2.609–74.641	3.089–34.771
Reflections collected	38549	31566	20462	50538
Independent reflections [R_{int}]	8233 [0.0533]	2562 [0.0342]	6297 [0.0582]	9734 [0.0428]
Data completeness (%)	99.7 to θ = 25.25°	99.8 to θ = 25.25°	98.6 to θ = 67.75°	99.3 to θ = 25.25°
Data/restraints/parameters	8233/0/254	2562/87/120	6297/0/362	9734/501/363
Goodness-of-fit on F^2	1.072	1.043	1.061	1.030
Final R for data with $I > 2\sigma(I)$	R_1 = 0.0465 wR_2 = 0.0754	R_1 = 0.0215 wR_2 = 0.0467	R_1 = 0.0632 wR_2 = 0.1806	R_1 = 0.0380 wR_2 = 0.0769
Final R for all data	R_1 = 0.0683 wR_2 = 0.0809	R_1 = 0.0297 wR_2 = 0.0504	R_1 = 0.0686 wR_2 = 0.1899	R_1 = 0.0658 wR_2 = 0.0862
Largest diff. peak/hole (e Å^{-3})	1.243/−0.771	0.347/−0.418	2.766/−2.170	1.455/−1.121
Extinction coefficient	0.0043(3)	0.00305(18)	0.00130(14)	0.0230(5)
Flack parameter	−0.021(12)	-	-	-

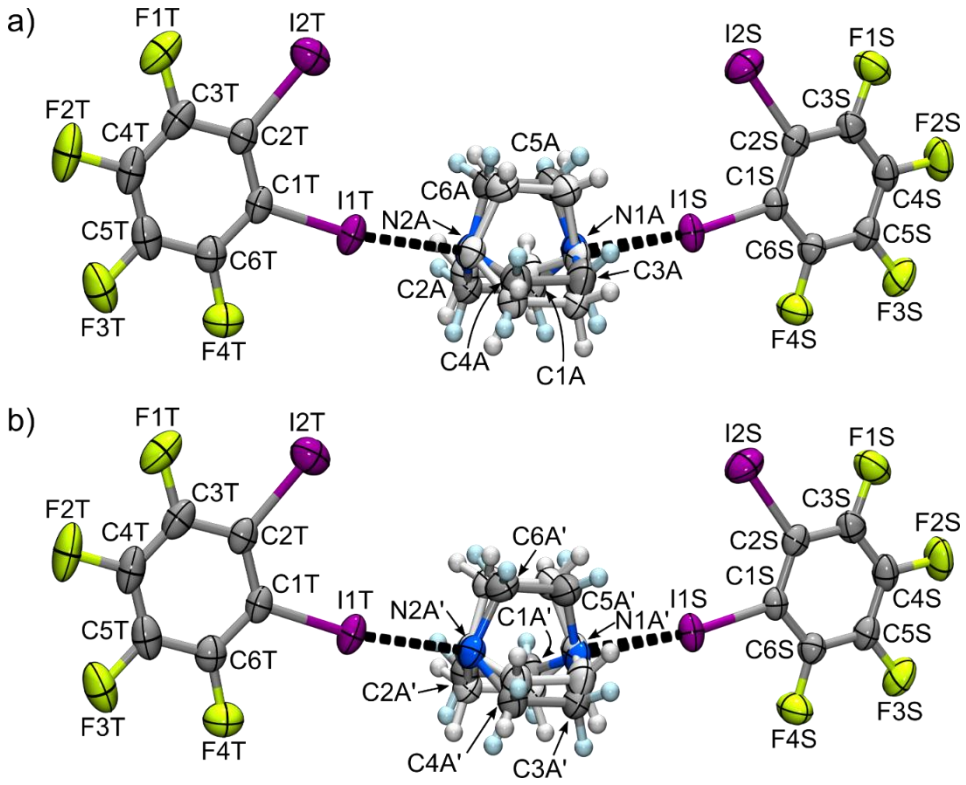

Fig. S8 Asymmetric unit of (**dabco**)(**12tfib**)$_2$ (collected at 253 K) showing the atom labelling scheme, presenting the labelling for the a) major and b) minor disorder component of **dabco**. Displacement ellipsoids are drawn at the 50 % probability level, halogen bonds are marked with black dashed lines, and H atoms are shown as small spheres of arbitrary radius.

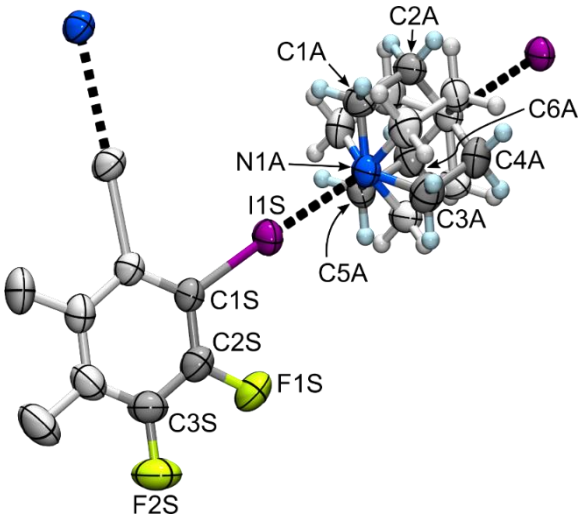

Fig. S9 Asymmetric unit of (**dabco**)(**12tfib**)-HT (collected at 253 K) showing the atom labelling scheme. Displacement ellipsoids are drawn at the 50 % probability level, halogen bonds are marked with black dashed lines, and H atoms are shown as small spheres of arbitrary radius.

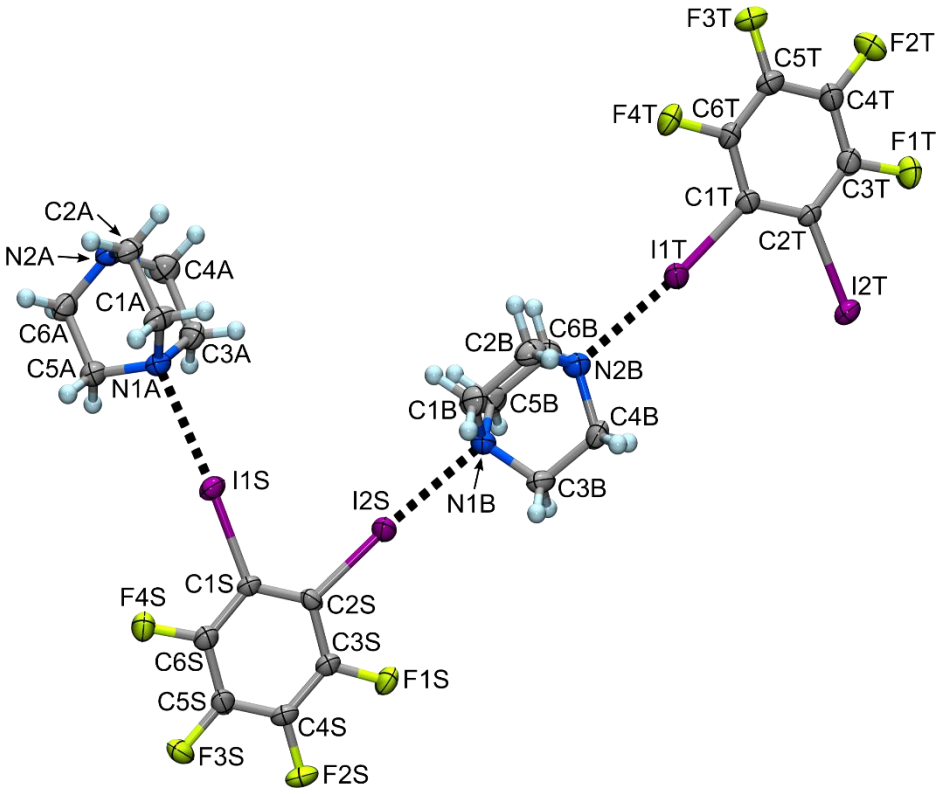

Fig. S10 Asymmetric unit of (**dabco**)(**12tfib**)-LT (collected at 173 K) showing the atom labelling scheme. Displacement ellipsoids are drawn at the 50 % probability level, halogen bonds are marked with black dashed lines, and H atoms are shown as small spheres of arbitrary radius.

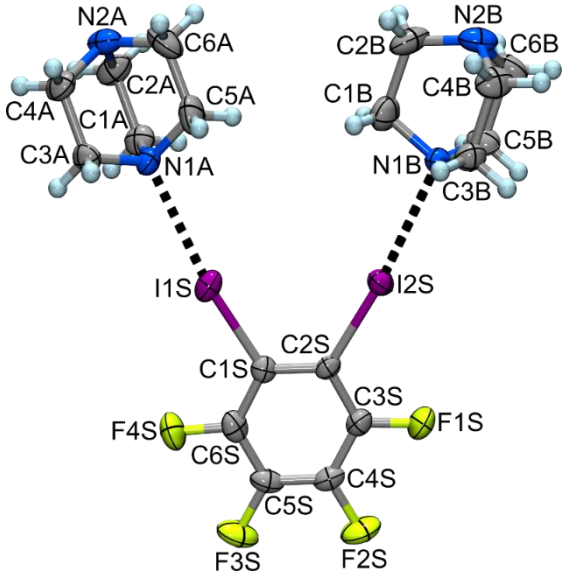

Fig. S11 Asymmetric unit of (**dabco**)$_2$(**12tfib**) (collected at 253 K) showing the atom labelling scheme. Displacement ellipsoids are drawn at the 50 % probability level, halogen bonds are marked with black dashed lines, and H atoms are shown as small spheres of arbitrary radius.

7. Thermal Analysis

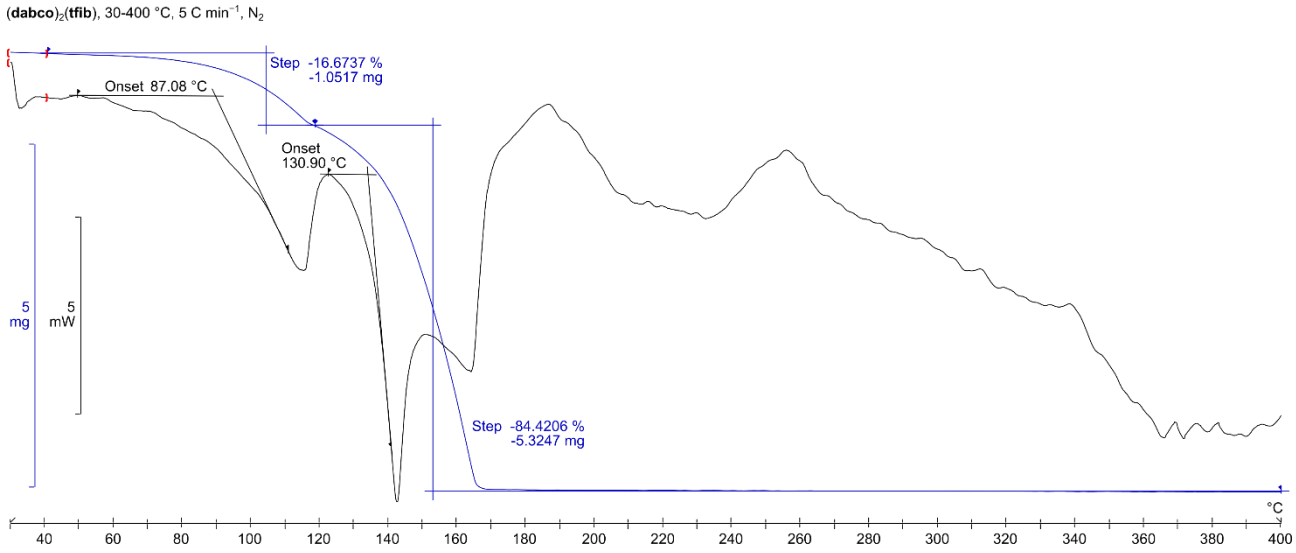

Fig. S12 TGA (blue) and DSC (black) curves for the cocrystal (**dabco**)$_2$(**12tfib**).

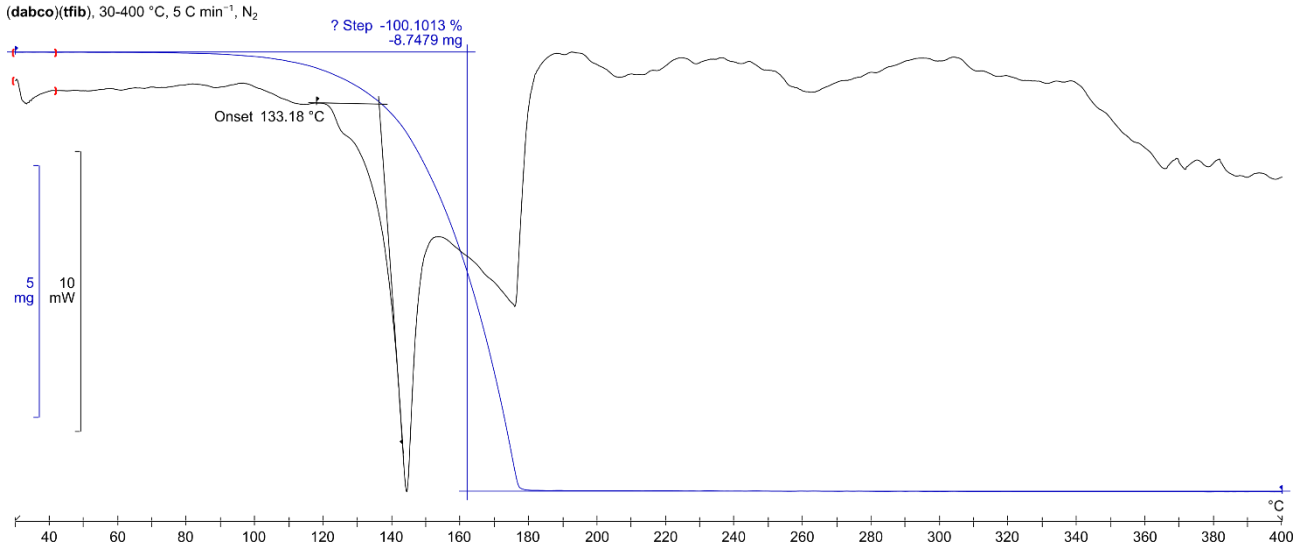

Fig. S13 TGA (blue) and DSC (black) curves for the cocrystal (**dabco**)(**12tfib**).

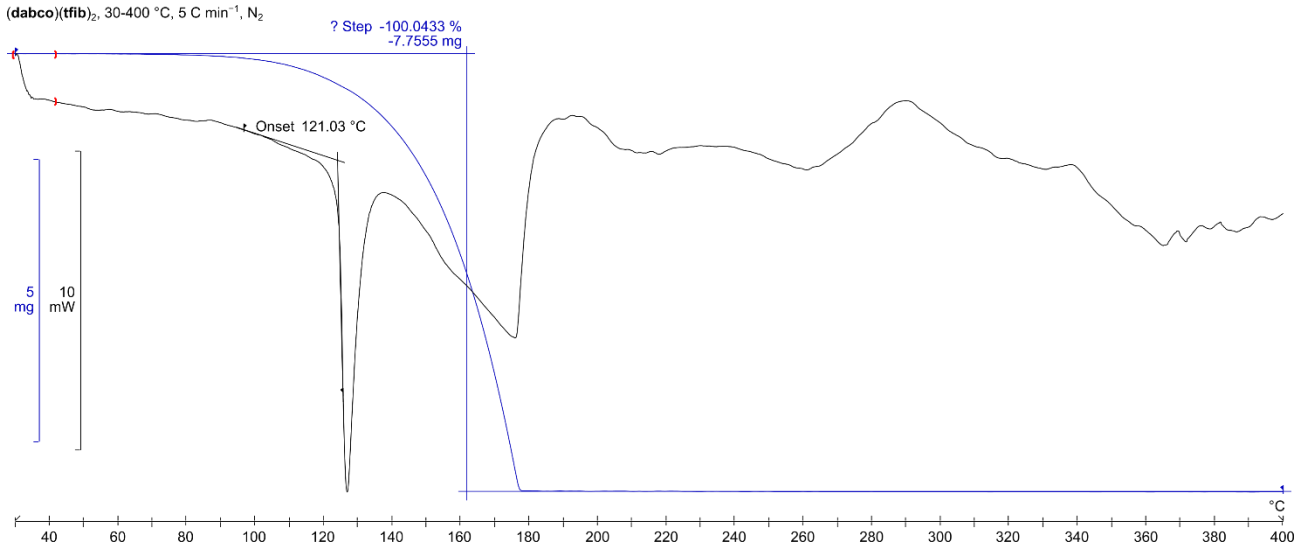

Fig. S14 TGA (blue) and DSC (black) curves for the cocrystal (**dabco**)(**12tfib**)$_2$.

8. References

1 TOPAS Academic 6.0, Coelho software, Brisbaine, Australia 2017.

2 STARe 16.0, Mettler Toledo, Columbus OH, USA 2018.

3 S. J. Clark, M. D. Segall, C. J. Pickard, P. J. Hasnip, M. I. J. Probert, K. Refson and M. C. Payne, *Z. Kristallogr.*, 2005, **220**, 567–570.

4 T. Björkman, *Comput. Phys. Commun.*, 2011, **182**, 1183–1186.

5 J. P. Perdew, K. Burke and M. Ernzerhof, *Phys. Rev. Lett.*, 1996, **77**, 3865–3868.

6 A. M. Reilly and A. Tkatchenko, *Chem. Sci.*, 2015, **6**, 3289–3301.

7 A. Ambrosetti, A. M. Reilly, R. A. DiStasio and A. Tkatchenko, *J. Chem. Phys.*, 2014, **140**, 18A508.

8 A. Tkatchenko, R. A. DiStasio, R. Car and M. Scheffler, *Phys. Rev. Lett.*, 2012, **108**, 236402.

9 S. Grimme, *J. Comput. Chem.*, 2006, **27**, 1787–1799.

10 A. Tkatchenko and M. Scheffler, *Phys. Rev. Lett.*, 2009, **102**, 073005.

11 W. Kohn and L. J. Sham, *Phys. Rev.*, 1965, **140**, A1133–A1138.

12 J. P. Perdew, A. Ruzsinszky, G. I. Csonka, O. A. Vydrov, G. E. Scuseria, L. A. Constantin, X. Zhou and K. Burke, *Phys. Rev. Lett.*, 2008, **100**, 136406.

13 H. J. Monkhorst and J. D. Pack, *Phys. Rev. B*, 1976, **13**, 5188–5192.

14 APEX3, Bruker AXS Inc., Madison, WI, USA, 2012.

15 L. Krause, R. Herbst-Irmer, G. M. Sheldrick and D. Stalke, *J. Appl. Crystallogr.*, 2015, **48**, 3–10.

16 G. M. Sheldrick, *Acta Crystallogr. Sect. A Found. Adv.*, 2015, **71**, 3–8.

17 G. M. Sheldrick, *Acta Crystallogr. Sect. C Struct. Chem.*, 2015, **71**, 3–8.

18 L. J. Farrugia, *J. Appl. Crystallogr.*, 2012, **45**, 849–854.

19 C. F. Macrae, I. J. Bruno, J. A. Chisholm, P. R. Edgington, P. McCabe, E. Pidcock, L. Rodriguez-Monge, R. Taylor, J. van de Streek and P. A. Wood, *J. Appl. Crystallogr.*, 2008, **41**, 466–470.

20 Persistence of Vision^{TM} Raytracer, Persistence of Vision Pty. Ltd., Williamstown, Victoria, Australia, 2004.